# Spin differences in the $^{90}$Zr compound nucleus induced by $(p,p')$, $(p,d)$, and $(p,t)$ surrogate reactions

S. Ota,[1,*] J. T. Harke,[1] R. J. Casperson,[1] J. E. Escher,[1] R. O. Hughes,[1] J. J. Ressler,[1] N. D. Scielzo,[1] I. J. Thompson,[1] R. A. E. Austin,[2] B. Abromeit,[3] N. J. Foley,[3] E. McCleskey,[3] M. McCleskey,[3] H. I. Park,[3] A. Saastamoinen,[3] and T. J. Ross[4]

[1]*Lawrence Livermore National Laboratory, Livermore, California 94551, USA*

[2]*Saint Mary's College, Halifax, Nova Scotia, Canada*

[3]*Cyclotron Institute, Texas A&M University, College Station, Texas 77840, USA*

[4]*Department of Chemistry, University of Kentucky, Lexington, Kentucky 40506, USA*

(Received 27 July 2015; published 4 November 2015)

The effect of the production mechanism on the decay of a compound nucleus is investigated. The nucleus $^{90}$Zr was produced by three different reactions, namely $^{90}$Zr$(p,p')^{90}$Zr, $^{91}$Zr$(p,d)^{90}$Zr, and $^{92}$Zr$(p,t)^{90}$Zr, which served as surrogate reactions for $^{89}$Zr$(n,\gamma)$. The spin-parity ($J^\pi$) distributions of the states populated by these reactions were studied to investigate the surrogate reaction approach, which aims at indirectly determining cross sections for compound-nuclear reactions involving unstable targets such as $^{89}$Zr. Discrete $\gamma$ rays, associated with transitions in $^{90}$Zr and $^{89}$Zr, were measured in coincidence with light ions for scattering angles of 25°–60° and $^{90}$Zr excitation energies extending above the neutron separation energy. The measured transition systematics were used to gain insights into the $J^\pi$ distributions of $^{90}$Zr. The $^{90}$Zr$(p,p')$ reaction was found to produce fewer $\gamma$ rays associated with transitions involving high spin states ($J = 6$–$8\ \hbar$) than the other two reactions, suggesting that inelastic scattering preferentially populates states in $^{90}$Zr that have lower spins than those populated in the transfer reactions investigated. The $\gamma$-ray production was also observed to vary by factors of 2–3 with the angle at which the outgoing particle was detected. These findings are relevant to the application of the surrogate reaction approach.

DOI: 10.1103/PhysRevC.92.054603 PACS number(s): 24.87.+y, 24.60.Dr, 25.85.Ec, 24.50.+g

## I. INTRODUCTION

Cross sections of neutron-induced reactions such as $(n,f)$, $(n,\gamma)$, and $(n,2n)$ at neutron energies ($E_n$) of a few tens of keV to a few tens of MeV are crucial inputs for nuclear energy applications [1], astrophysical studies [2,3], and radiochemical applications [4–6]. However, the cross sections for most short-lived isotopes remain poorly known because of their inaccessibility as target materials. During the past decade, the importance of these compound-nuclear reaction cross sections for applications has led to renewed interest in indirect methods, such as the surrogate reactions approach [7]. This method aims at determining neutron-induced reaction cross sections by accessing the compound nuclei of interest via alternative reactions such as transfer reactions or inelastic scattering involving stable beams and targets. In a surrogate experiment, a direct reaction is employed to produce a highly excited nuclear system, which is assumed to subsequently equilibrate to form the same compound nucleus that appears in the (desired) neutron-induced reaction. The outgoing particle from the initial reaction is detected in coincidence with an observable (e.g., a specific $\gamma$-ray transition or fission fragments) that is characteristic of the decay channel of interest and the measured coincidence probability is used to determine or constrain the reaction cross section. While the applicability of the surrogate reaction approach has been successfully demonstrated for $(n,f)$ cross sections (e.g., [8–13]), it has been difficult to determine $(n,\gamma)$ cross sections (e.g., [14–16]).

A primary difficulty in determining $(n,\gamma)$ cross sections is the difference in the spin-parity ($J^\pi$) distributions of the compound nucleus created by the $(n,\gamma)$ and the surrogate reactions. While this has a smaller effect on the extraction of fission cross sections [9], the $\gamma$-ray emission of the compound nucleus can be quite sensitive to the initial $J^\pi$ distribution [14,15,17–20]. Therefore, in order to extract $(n,\gamma)$ cross sections from surrogate data it becomes necessary to take into account the $J^\pi$ distribution of the decaying compound nucleus. When this distribution is known, the decay of the nucleus can be modeled and constraints on the desired $(n,\gamma)$ cross sections are obtained by fitting the decay model to observables from the surrogate experiment. Preliminary work on the $A = 155$–$158$ gadolinium isotopes, for which structure information, as well as high quality directly measured cross sections are available (see [15] and references therein), indicates that accounting for $J^\pi$ differences between the desired $(n,\gamma)$ and surrogate reactions can yield significant improvements for the extracted cross section [21].

The $^{90}$Zr nucleus is well suited for further benchmarking of this surrogate approach. The presence of closed proton ($Z = 40$) and neutron ($N = 50$) (sub)shells in the Zr mass region ($A \sim 90$) is manifest in the low level densities in the nuclei studied. This, in turn, leads to a competition between $\gamma$ decay and neutron emission that is quite sensitive to the $J^\pi$ distributions of the decaying compound nuclei and can be expected to be visible in the measured discrete $\gamma$-ray emission probabilities [7,14,17]. The effect is smaller in well-deformed nuclei with high level densities, such as rare-earth and actinide nuclei that have been studied in [15,22]. Additionally, investigating the $^{90}$Zr nucleus also has the advantage that the nuclear structure of $^{90}$Zr and neighboring nuclei have been

*ota2@llnl.gov

 

extensively studied. Finally, the $^{90}$Zr can be produced by multiple different reaction mechanisms since there are several stable Zr isotopes. The data obtained in this study are expected to aid in the determination of the $^{89}$Zr$(n,\gamma)$ cross section, which, due to the short half-life of 3.27 days, has not been measured directly.

The implementation of the surrogate approach for $(n,\gamma)$ reactions typically relies on experimentally measured emission probabilities ($P_i$) of various discrete $\gamma$ rays ($i$) from the compound nucleus. While these observables are important for constraining $(n,\gamma)$ calculations, they can also be employed to provide information on the $J^\pi$ distributions of the decaying nucleus. In the present work, we employ $P_i$ to obtain insights into the $J^\pi$ distributions of the $^{90}$Zr nucleus produced in several different reactions. Specifically, we compare $P_i$ for $\gamma$-ray transitions in $^{90,89}$Zr, following the production via inelastic $(p,p')$,$(p,p'n)$ scattering, and $(p,d)$,$(p,dn)$ and $(p,t)$,$(p,tn)$ transfer reactions. Earlier studies suggest that the direct reactions typically used in surrogate experiments transfer more units of angular momentum ($\Delta L$) to the compound nucleus than the neutron does in the desired reaction [15,20,23]. For $^{158}$Gd, it was estimated that $(p,d)$ and $(p,t)$ reactions transfer $\Delta L = 4\hbar$ and $\Delta L = 5\hbar$, respectively, in the quasi-continuum region ($E_x = 3.5$–$5$ MeV) [23], and describing the data obtained in inelastic proton scattering on gadolinium seems to require similarly large $\Delta L$ transfers. These values are significantly larger than the $\Delta L < 2\hbar$ typically transferred in low-energy $(n,\gamma)$ reactions [14,15]. Thus investigating the effect of the production mechanism on the decay of a compound nucleus is of great help for developing the surrogate reaction approach.

In a surrogate analysis that takes into account the $J^\pi$ distribution of the compound nucleus, $P_i(E_x)$ for various discrete $\gamma$ rays as a function of the excitation energy ($E_x$) are predicted. This requires a description of the surrogate reaction mechanism that yields the $J^\pi$ distribution $F^{CN}(E_x,J^\pi)$ of the compound nucleus as a function of $E_x$ and angle of the outgoing particle (for simplicity the latter is suppressed in the equations here), as well as a rough decay model that approximately describes the decay of the compound nucleus $[G^{CN}(E_x,J^\pi)]$. A Hauser-Feshbach-type calculation is then carried out to predict the relevant $\gamma$ decay probabilities:

$$P_i(E_x) = \Sigma_{J,\pi} F^{CN}(E_x,J^\pi) G^{CN}(E_x,J^\pi). \quad (1)$$

Adjusting the parameters that enter the $G^{CN}(E_x,J^\pi)$ in order to fit the calculated decay probabilities to surrogate data $[P_i(E_x)]$ then provides constraints on the nuclear structure properties (level densities, $\gamma$-ray strength functions, etc.) employed in the decay model. The decay model constrained in this manner can then be used to calculate the cross section $[\sigma_{(n,\gamma)}(E_n)]$ of the desired neutron-induced reaction with the calculated compound nucleus formation cross section $[\sigma^{CN}(E_x,J^\pi)]$ by

$$\sigma_{(n,\gamma)}(E_n) = \Sigma_{J,\pi} \sigma^{CN}(E_x,J^\pi) G^{CN}(E_x,J^\pi), \quad (2)$$

where $E_n = [(A_{\text{target}}+1)/A_{\text{target}}] \times (E_x - S_n)$ and therefore $E_n \approx E_x - S_n$ for $^{90}$Zr (mass of target nucleus $A_{\text{target}} = 90$), and $S_n = 11.97$ MeV for $^{90}$Zr. Thus to obtain useful constraints on modeling, it is important to experimentally determine $P_i(E_x)$ for multiple $\gamma$-ray transitions in the decay following the population of $^{90}$Zr around $S_n$ and above.

TABLE I. Isotopic composition of $^{90,91,92}$Zr targets (%).

| Mass number | $^{90}$Zr | $^{91}$Zr | $^{92}$Zr |
|---|---|---|---|
| 90 | 99.36 | 6.51 | 2.86 |
| 91 | 0.30 | 88.50 | 1.29 |
| 92 | 0.17 | 3.21 | 94.57 |
| 94 | 0.12 | 1.61 | 1.15 |
| 96 | 0.04 | 0.17 | 0.14 |

As the $P_i(E_x)$ depend on the $J^\pi$ distribution of the decaying compound nucleus, they provide not only constraints for the Hauser-Feshbach decay model, but also information that gives useful insights into the reaction mechanisms that created the compound nucleus. Specifically, the deexcitation of the compound nucleus is expected to proceed via the emission of only a few (1–3) transitions, which are predominantly of $E1$ character. We expect that transitions that increase $J$ are approximately as likely as transitions that decrease $J$. Thus, distributions of the measured discrete $\gamma$-ray transitions are expected to reflect the characteristics of the $J^\pi$ distribution with which the compound nucleus was initially produced. The measured transition systematics are used to gain insights into the $J^\pi$ distributions of $^{90}$Zr produced by the three different reaction types studied [$^{90}$Zr$(p,p')$, $^{91}$Zr$(p,d)$, and $^{92}$Zr$(p,t)$].

## II. EXPERIMENT

The experiments were performed at the K150 Cyclotron facility at Texas A&M University. Enriched $^{90,91,92}$Zr targets (1.02, 1.01, and 0.960 mg/cm$^2$, respectively) were bombarded with a 28.56-MeV proton beam with an intensity of about 1.5 nA. Measurements using the $^{90,91,92}$Zr targets were made for 12, 36, and 84 hours, respectively. Since these targets contain other Zr isotopes as shown in Table I, additional measurements using enriched $^{94,96}$Zr targets (0.960 and 0.976 mg/cm$^2$) were made in order to subtract their contributions. In addition, each target had a small amount of carbon and oxygen. Data was therefore collected using a natural C target (0.1 mg/cm$^2$), which contains oxygen as a contaminant, to estimate carbon and oxygen backgrounds in the targets. Details of the procedure to subtract the backgrounds can be found in [15,24].

The energy spectra and angular distribution of the light ions and prompt $\gamma$-rays were measured with the Silicon Telescope Array for Reaction studies, Livermore, Texas, Richmond (STARLiTeR) detector system [25]. STARLiTeR consists of three segmented Micron S2 silicon detectors [26] (referred to $\Delta E, E1$, and $E2$) which are each segmented into 24 rings and 8 wedges, allowing the measurement of charged-particle scattering angles. The thicknesses of the $\Delta E$, $E1$, and $E2$ detectors are 143, 1000, and 994 $\mu$m, respectively. The $\Delta E$, $E1$, and $E2$ detectors were located at 19.2, 23.4, and 33.8 mm from the target and were used to identify charged particles from $(p,p')$, $(p,d)$, and $(p,t)$ reactions covering angles between 31° and 56° for measurements by $\Delta E + E1$, and between 31° and

46° for ones by $\Delta E + E1 + E2$. However, the actual angular coverage spanned 25°–58° and 25°–48°, respectively, since the beam position in the present experiment was found to be displaced ∼2.6 mm from the center of the detector array. This was determined by studying the spatial dependence of the kinematic shifts observed in the C target data as was done in [15]. The particle events were recorded when both the $\Delta E$ and the $E1$ detectors were hit.

For $\gamma$-ray detection, five bismuth germanate (BGO) Compton-suppressed high-purity germanium (HPGe) clover detectors surrounded the silicon chamber (see e.g., [15,25]). The energy resolution and the total absolute photopeak efficiency ($\epsilon$) were measured using calibrated $\gamma$-ray sources placed at the target position before and after the experiments. The typical energy resolution was 2 keV for energies below 500 keV, increasing to 5 keV at 3 MeV. The efficiency, $\epsilon$, of the array was 3.8% at 150 keV, 1.5% at 500 keV, and 0.5% at 2 MeV after add-back was applied.

Coincident particle-$\gamma$ events were identified based on the time difference between particle and prompt $\gamma$-ray signals. Typical timing gates were set between +500 ns and −125 ns around the time difference peak. This window is sufficiently wide to include most decays from the 3559 keV ($8^+$) state in $^{90}$Zr nuclei which has a lifetime of 131 ns [27].

Further details on the detector arrays, data-taking system, and data analysis can be found in [12,24,28].

## III. EXCITATION SPECTRA AND DISCRETE $\gamma$-RAY MEASUREMENTS

### A. Excitation spectrum

After particle identification (PID) using a conventional $\Delta E$-range plot (see [24]), about $5\times10^7$ proton, $2\times10^7$ deuteron, $6\times10^6$ triton singles events were collected from $^{90}$Zr$(p,p')$, $^{91}$Zr$(p,d)$, and $^{92}$Zr$(p,t)$ reactions, respectively. The detected particle energy was corrected for the recoil energy of the target nuclei and energy losses in the targets and dead layers (∼200 $\mu$g/cm$^2$ Al and ∼1 mg/cm$^2$ Au) of the Si detectors to obtain the total kinematic energy ($E$). The excitation energies ($E_x$) in $^{90}$Zr can then be determined from $E_x = E_b - E + Q$, where the beam energy $E_b = 28.56$ MeV, and $Q$ values for $(p,p')$, $(p,d)$, and $(p,t)$ reactions are 0, −4.969, and −7.346 MeV, respectively.

Figure 1 shows the observed $E_x$ distribution for $^{90}$Zr produced by the $^{90}$Zr$(p,p')$, $^{91}$Zr$(p,d)$, and $^{92}$Zr$(p,t)$ reactions after correcting for backgrounds from the Zr, C, and O contaminants. The full-width at half maximum (FWHM) energy resolution for the $^{91}$Zr$(p,d)$ ground state peak measured by the $\Delta E + E1 + E2$ detectors was ∼300 keV. Similarly, the energy resolution for the $^{92}$Zr$(p,t)$ ground state peak measured by the $\Delta E + E1$ detectors was ∼200 keV.

In the $^{90}$Zr$(p,p')$ reaction, events with $E_x < 7$ MeV were mostly missed because these particles punch through even the $E2$ detector. On the high energy side, the events with $E_x > 21$ MeV were mostly cut off because these are stopped in the $\Delta E$ detector. Therefore, the energy range utilized in the $^{90}$Zr$(p,p')$ reactions is $E_x = 7.0$–$21.0$ MeV, which spans a 14-MeV energy region around the neutron separation energy of

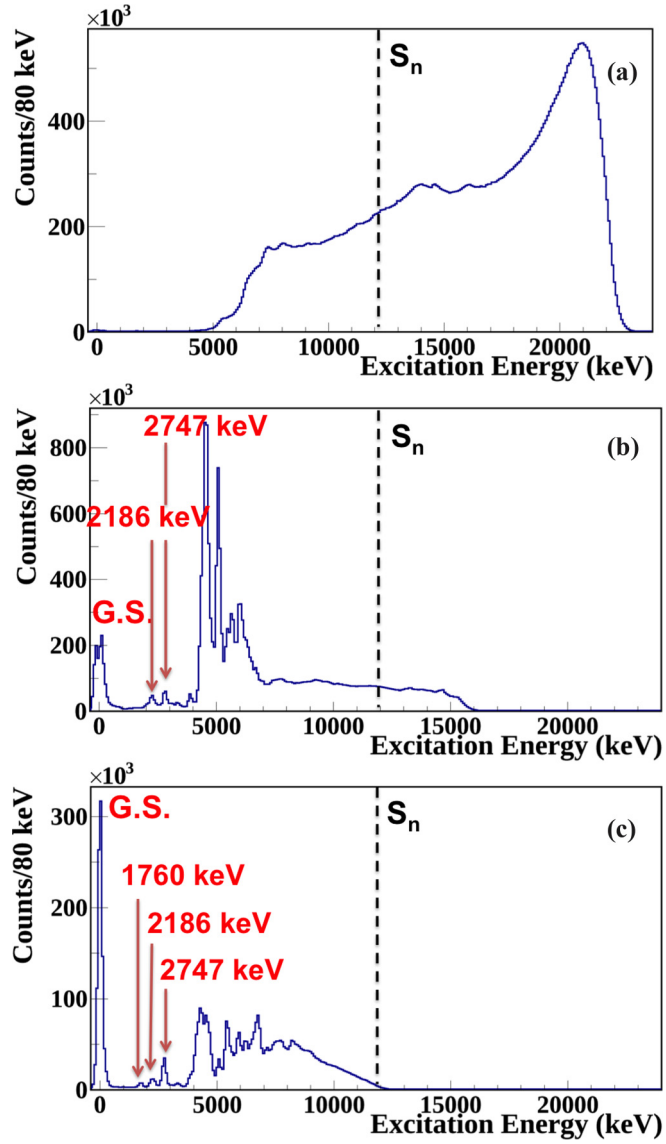


FIG. 1. (Color online) Total particle spectra as a function of excitation energy in $^{90}$Zr from (a) $^{90}$Zr$(p,p')$, (b) $^{91}$Zr$(p,d)$, and (c) $^{92}$Zr$(p,t)$ reactions.

$^{90}$Zr ($S_n = 11.97$ MeV). Likewise, the energy ranges utilized in $^{91}$Zr$(p,d)$ and $^{92}$Zr$(p,t)$ reactions are $E_x = 0$–15 MeV and $E_x = 0$–11 MeV, respectively. These are wide enough to study excitations around $S_n$ although the energy region above $S_n$ is missed in the $^{92}$Zr$(p,t)$ reactions. Additionally, it should be mentioned that the shapes of the proton spectrum for $E_x$ below 13.5 MeV and the deuteron spectrum for $E_x$ below 3 MeV are influenced by the angular acceptance of the detector setup as the measurement of the full energy for the highest energy particles requires the $E2$ detector. However, these influences on the following analysis are negligibly small.

From Figs. 1(b) and 1(c), we can observe some levels with $E_x < 4$ MeV are observed in $^{91}$Zr$(p,d)$ and $^{92}$Zr$(p,t)$ reactions. In both reactions, $E_x = 2.186$ MeV ($2^+$) and 2.747 MeV ($3^-$) states were clearly observed. The first and third excited states [$E_x = 1760$ keV ($0^+$) and 2.319 MeV ($5^-$)]

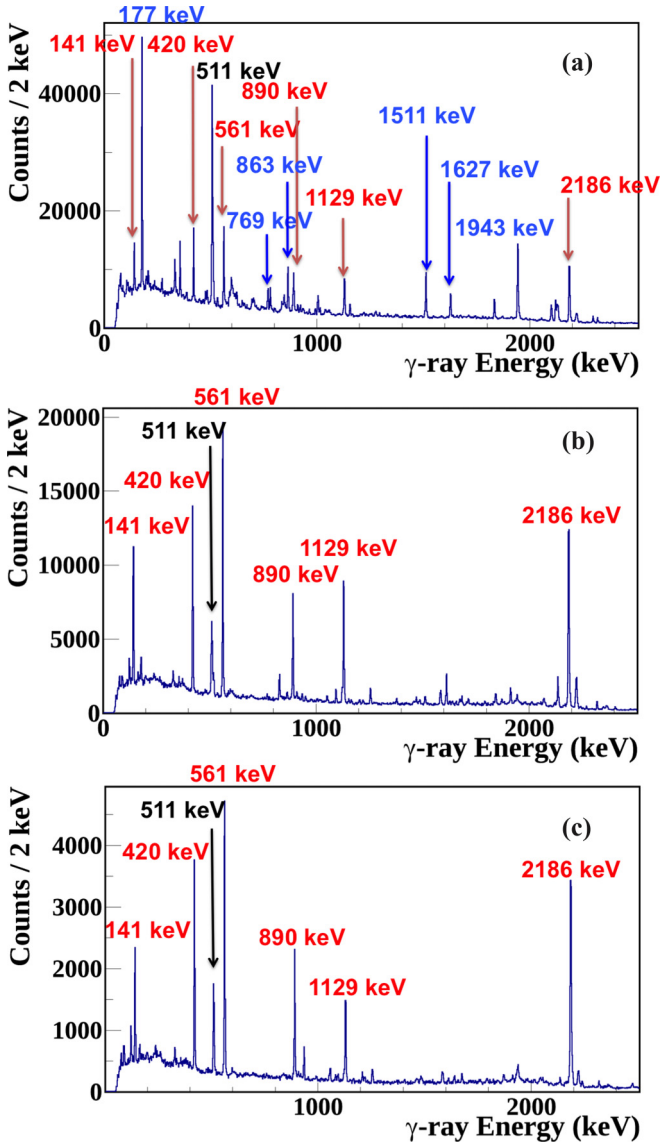


FIG. 2. (Color online) Total $\gamma$-ray spectra in coincidence with particles from (a) $^{90}$Zr$(p,p')$, (b) $^{91}$Zr$(p,d)$, and (c) $^{92}$Zr$(p,t)$ reactions. The intense $\gamma$ rays from $^{90}$Zr are marked in red. The $\gamma$ rays labeled in blue are from $^{89}$Zr.

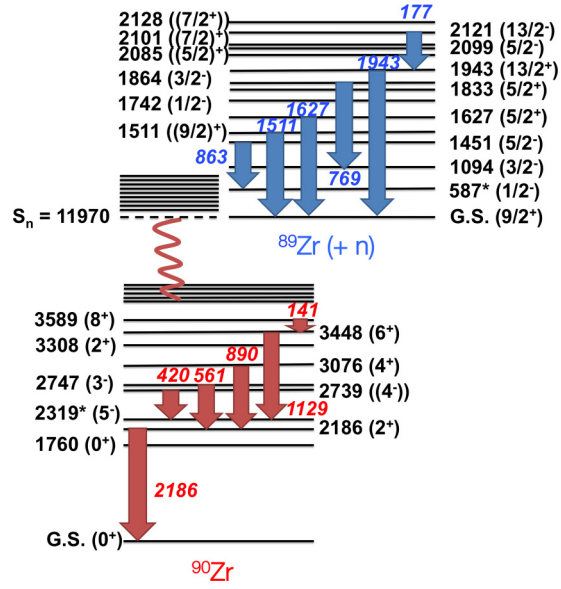


FIG. 3. (Color online) Discrete $\gamma$-ray transitions from $^{90}$Zr and $^{89}$Zr studied in the present work. The energies are shown in keV. $J^{\pi}$ of levels are given in parentheses and double parentheses means that there are uncertainties in assignment. The levels marked by $*$ are isomeric states from which $\gamma$ rays are unobservable in the present measurements.

were observed only in the $^{92}$Zr$(p,t)$ reaction. These results agree well with previous $^{91}$Zr$(p,d)$ [29] and $^{92}$Zr$(p,t)$ [30] measurements. Several large peaks are observed around $E_x =$ 4.0–7.0 MeV in both transfer reactions. Although the limited energy resolution of the Si detectors and high level densities do not allow for unambiguous structure information on these large peaks, the particle-$\gamma$ coincidence technique reveals the individual levels contributing to these peaks as described later.

### B. Discrete $\gamma$-ray measurements

The $\gamma$-ray energies were measured up to 5 MeV. The total spectra of $\gamma$ rays in coincidence with light ions are shown up to 2.5 MeV in Fig. 2. Contributions from contaminants in the targets are removed from these spectra. These background subtractions are sometimes important because, e.g., $^{91}$Zr$(p,p'n\gamma)$ may contaminate the true $^{90}$Zr$(p,p'\gamma)$ events as well as $\gamma$ rays with the close energy from $(p,p'\gamma)$ reactions of the contaminants [15].

In Fig. 2, the $\gamma$-ray spectra have many discrete $\gamma$-ray peaks from $^{90}$Zr in common. In Fig. 2(a), some discrete $\gamma$-ray peaks from $^{89}$Zr formed by the $^{90}$Zr$(p,p'n)$ reaction are also observable. These peaks can be observed in Fig. 2(b) although their intensities are smaller. The peaks shown in Fig. 2 are used in the data analysis and the level schemes associated with $^{89,90}$Zr are summarized in Fig. 3. The $0^+ \rightarrow 0^+$ transition from the first excited state at 1760 keV to the ground state, which contributes to the 511-keV annihilation peak in Fig. 2, was not used in the present study.

### C. Comparison with previous $(p,d)$ and $(p,t)$ measurements

The particle-$\gamma$ coincidence technique helps identify the levels where $\gamma$ rays originate, allowing some unresolved peaks in the particle spectra to be resolved with the precision of $\gamma$-ray detectors (<1 keV for centroid). By utilizing this approach and taking advantage of detailed knowledge of the $^{90}$Zr level scheme [31], contributions to the peak at $E_x \sim 4.5$ MeV in Fig. 1(b) are found to be $E_x = 4.541$ ($6^+$, 26%), 4.454 ($5^+$, 24%), 4.331 ($3^+$, 17%), 4.814 and 4.818 [$3^-$, and $(3,4)^+$, 11% for the sum], and 4.640 MeV [(7,8), 10%] levels (percentage denotes contributions to the peak). Likewise, it was found that the peak at $E_x \sim 5.0$ MeV consists of $E_x = 5.060$ ($7^+$, 56%), 4.992 ($2^-$, 22%), 5.107 MeV [$(3,4)^+$, 15%] levels. These can be compared with a previous $^{91}$Zr$(p,d)$ measurement which was performed at 30° with a 31-MeV proton beam [29]. Comparing to the intense peaks of $E_x = 4.320$, 4.443,

4.528, 5.050 MeV reported by [29], these correspond to $E_x = 4.331$, 4.454, 4.541, 5.060 MeV found in the present spectrum. Therefore, the present experiment agrees quite well with the past $^{91}$Zr$(p,d)$ experiment except for a ∼10-keV calibration offset present in the previous work.

The same approach can be applied for Fig. 1(c). It turned out that the peak at $E_x \sim 4.5$ MeV consists of $E_x = 4.331$ ($4^+$, 18%), 4.541 ($6^+$, 18%), 4.124 ($0^+$, 16%), 4.229 ($2^+$, 10%), 4.681($2^+$, 10%), 4.814, and 4.818 [$3^-$ and $(3,4)^+$, 5% for the sum] MeV levels (percentage denotes contribution to the peak). The peak at $E \sim 5.1$ MeV mostly consists of $E_x = 5.060$ MeV ($7^+$) and the peak at ∼5.5 MeV consists of $E_x = 5.457$ ($4^+$, 17%) and 5.513 MeV [$(3,4)^-$, 15%].

These structures can be compared with the $^{92}$Zr$(p,t)$ spectrum from Ball *et al.* [30] which was measured at 20° using a 38-MeV proton beam. The intense peaks reported from that experiment are 4.125, 4.232, 4.335, 4.543, 4.683, and 5.441 MeV. These agree well with the peaks at 4.124, 4.229, 4.331, 4.541, 4.681, and 5.457 MeV in the present $^{92}$Zr spectrum.

Further details of the results shown in the present section will be found in [32].

## IV. GAMMA DECAY PROBABILITIES FROM INELASTIC AND TRANSFER REACTIONS

### A. Definition of γ decay probability

We are interested in the the probability that the compound nucleus of interest (here $^{90}$Zr), produced at a particular excitation energy $E_x$, decays via a specific $\gamma$-ray transition ($i$) that can be experimentally observed. This $\gamma$ decay probability is given by

$$P_i(E_x) = \frac{(1+\alpha_{IC})N_{P\text{-}\gamma}(E_x,i)}{\epsilon(E_\gamma)N_{\text{singles}}(E_x)}\,, \tag{3}$$

where $N_{\text{singles}}$ gives the number of single events (outgoing direct-reaction particle observed in detector), $N_{P\text{-}\gamma}$ is the number of particle-$\gamma$ coincidences observed for the transition of interest, $\epsilon$ denotes the $\gamma$-ray detection efficiency at the $\gamma$-ray energy $E_\gamma$, and $\alpha_{IC}$ gives the relevant internal conversion coefficient. $N_{\text{singles}}(E_x)$ is obtained from Fig. 1, while $N_{P\text{-}\gamma}(E_x)$ is obtained from the $\gamma$-ray spectrum gated on $E_x$ by fitting a specific peak assuming a Gaussian shape. $\alpha_{IC}$ for the individual $\gamma$ rays were calculated using the software BRICC V. 2.0B [33].

### B. Reaction dependence

Figure 4 shows $P_i(E_x)$ for the six discrete $\gamma$-ray transitions from $^{90}$Zr low-lying states around $E_x = 2$–4 MeV (see Fig. 3) as a function of excitation energies up to $E_x = 20$ MeV. The $P_i(E_x)$ typically show some peaks at low excitation energies which correspond to direct population of levels which decay via these $\gamma$-ray transitions. In the region of 7 MeV $< E_x < S_n$, the level density is so high that the highly excited nuclear system that is produced in the surrogate (transfer or inelastic scattering) reaction mixes with the surrounding states and equilibrates, i.e., becomes a compound nucleus. We observe that the $P_i(E_x)$ are nearly constant in this high energy region. At excitation energies above $S_n$, the $P_i(E_x)$ drop to nearly zero because of the competition from neutron emission.

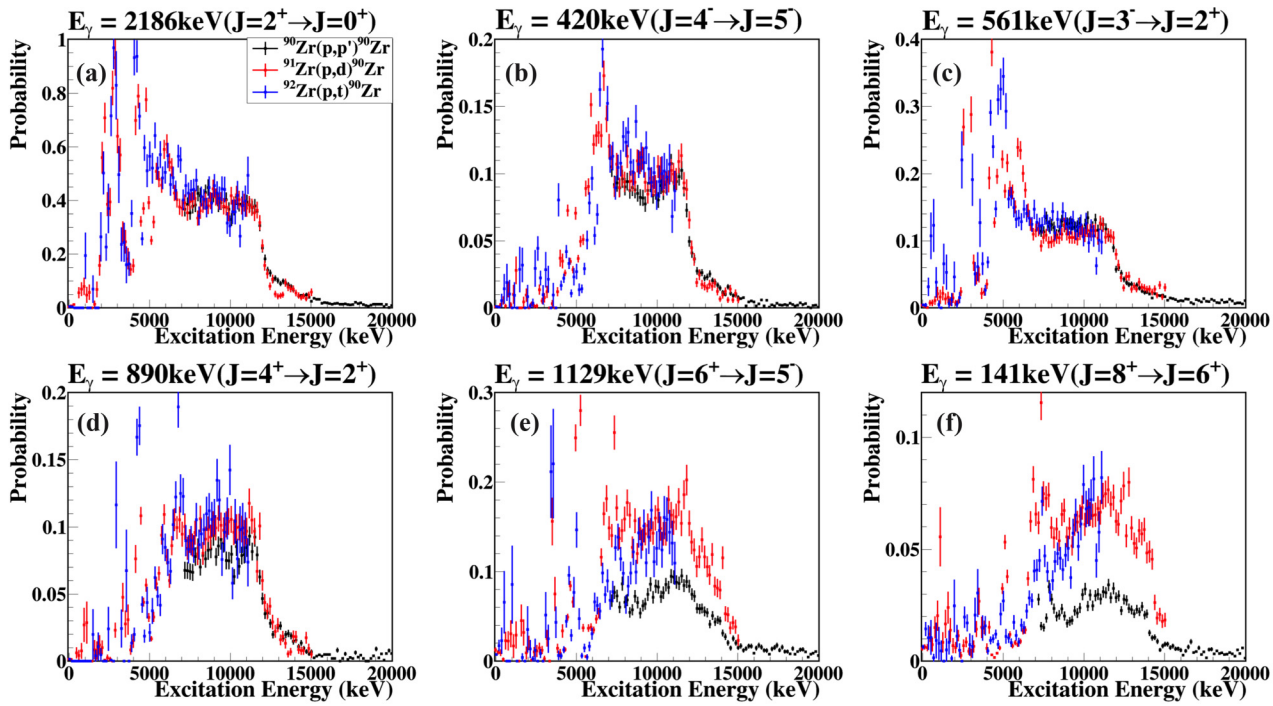


FIG. 4. (Color online) $\gamma$ decay probabilities as a function of $^{90}$Zr excitation energy for discrete $\gamma$-ray transitions from the $^{90}$Zr. (a) $E_\gamma = 2186$ keV, (b) 420 keV, (c) 561 keV, (d) 890 keV, (e) 1129 keV, and (f) 141 keV.

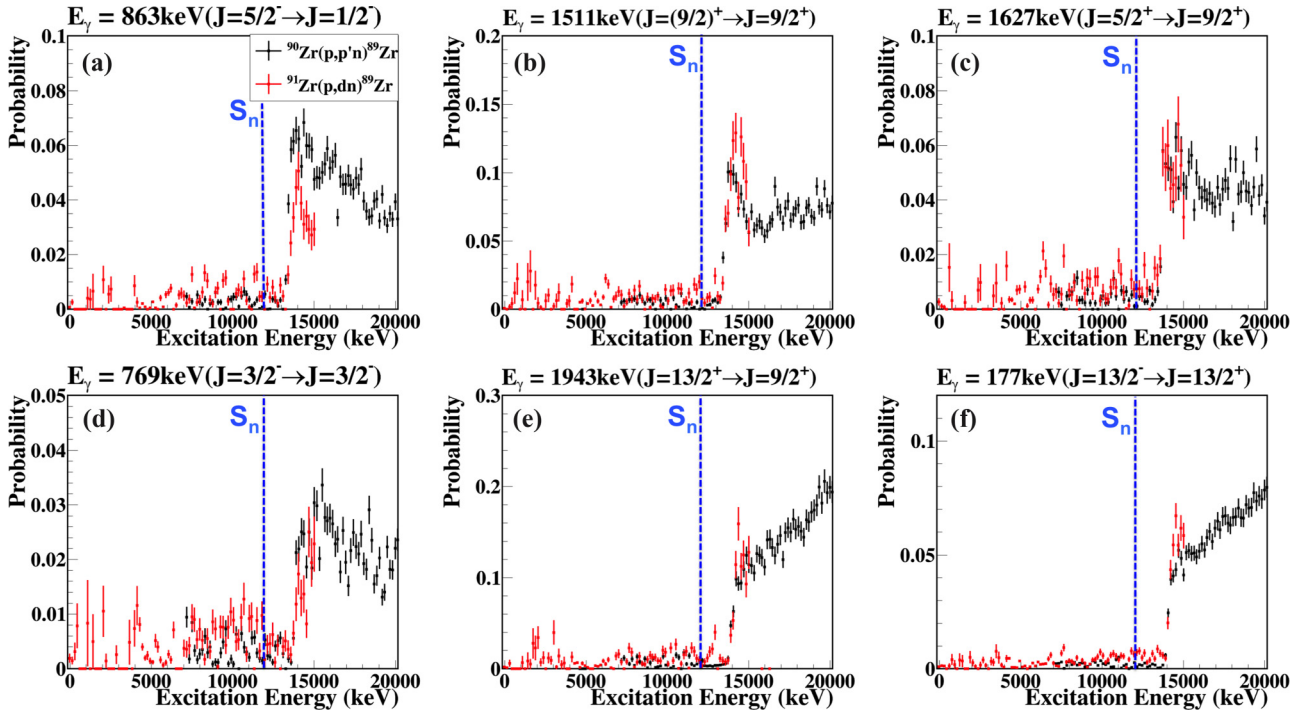


FIG. 5. (Color online) $\gamma$ decay probabilities as a function of $^{90}$Zr excitation energy for selected discrete $\gamma$-ray transitions between states of the $^{89}$Zr. (a) $E_\gamma = 863$ keV, (b) 1511 keV, (c) 1627 keV, (d) 769 keV, (e) 1943 keV, and (f) 177 keV.

The strongest $\gamma$-ray transition is 2186 keV from $(2^+ \rightarrow 0^+)$. Its $P_i(E_x)$ at the continuum region are about 0.4 for each reaction. The transitions from low $J$ states such as the 420 keV $(4^- \rightarrow 2^+)$, 561 keV $(3^- \rightarrow 2^+)$, 890 keV $(4^+ \rightarrow 2^+)$ $\gamma$-ray transitions show a similar trend indicating that the $P_i(E_x)$ are nearly independent of the reaction. The transitions from the higher $J$ states, 1129 keV $(6^+ \rightarrow 5^-)$ and 141 keV $(8^+ \rightarrow 6^+)$, show significant reaction dependence and $^{90}$Zr$(p,p')$ shows notably smaller $P_i(E_x)$ than the other two reactions. Given that the number of transitions from the continuum region to these low-lying levels are likely only one or a few $E1$ transitions and transitions that increase $J$ are approximately as likely as transitions that decrease $J$, the $J$ of the initial level of these measured discrete $\gamma$-ray transitions are expected to reflect the characteristics of the $J^\pi$ distribution with which the compound nucleus was initially produced. Therefore, these results strongly suggests that $^{90}$Zr$(p,p')$ does not populate as many high $J$ ($\geqslant 6\hbar$) states as $^{91}$Zr$(p,d)$ and $^{92}$Zr$(p,t)$ reactions.

Figure 5 shows $P_i(E_x)$ for the $\gamma$-ray transitions from $^{89}$Zr (see Fig. 3) produced by $^{90}$Zr$(p,p'n)$ and $^{91}$Zr$(p,dn)$ as a function of $E_x$ in $^{90}$Zr [the $^{92}$Zr$(p,t)$ data did not extend above $S_n$]. $P_i(E_x)$ for $\gamma$-ray transitions in $^{89}$Zr start to rise as the states become energetically accessible. The $P_i(E_x)$ above $S_n$ show $J$ dependence as was observed below $S_n$. $^{90}$Zr$(p,p'n)$ shows lower $P_i(E_x)$ than $^{91}$Zr$(p,dn)$ at high $J$ states ($J^\pi = 9/2^+$, $13/2^+$, and $13/2^-$). On the other hand, the $^{90}$Zr$(p,p'n)$ shows higher $P_i(E_x)$ than $^{91}$Zr$(p,dn)$ in $\gamma$-ray transitions from low $J$ states such as $5/2^-$ and $3/2^-$.

Figure 6 summarizes the angular momentum ($L$) dependence of $P_i(E_x)$ for each reaction below and above $S_n$. The $\gamma$ decay probability ratios of $^{90}$Zr$(p,p')$ and $^{92}$Zr$(p,t)$ relative to $^{91}$Zr$(p,d)$ below $S_n$, $R_{i,(p,p')/(p,d)}$ and $R_{i,(p,t)/(p,d)}$ are defined as follows and plotted in Fig. 6(a):

$$R_{i,(p,p')/(p,d)} = P_{i,(p,p')}/P_{i,(p,d)}, \tag{4}$$

$$R_{i,(p,t)/(p,d)} = P_{i,(p,t)}/P_{i,(p,d)}, \tag{5}$$

where $P_{i,(p,p')}, P_{i,(p,d)}$, and $P_{i,(p,t)}$ are average $P_i(E_x)$ at $E_x = 10.0$–$11.0$ MeV for $(p,p')$, $(p,d)$, and $(p,t)$ reactions, respectively. Likewise, the $\gamma$ decay probability ratios above $S_n$, $R_{i,(p,p'n)/(p,dn)}$ is defined by using $P_{i,(p,p'n)}$ and $P_{i,(p,dn)}$ which are average $P_i(E_x)$ at $E_x = 14.0$–$15.0$ MeV for $(p,p'n)$ and $(p,dn)$ reactions, respectively, and are plotted in Fig. 6(b).

Furthermore, the data from two and five more $\gamma$-ray transitions are added to Figs. 6(a) and 6(b), respectively (see the caption of Fig. 6). $L$ values are obtained from the $J^\pi$ of the decay levels. From Fig. 6(a), we can confirm that the probability ratio of $^{90}$Zr$(p,p')$ decreases as $L$ increases, while the probability ratio of $^{92}$Zr$(p,t)$ reaction stays about unity below $S_n$. Similarly, above $S_n$ the probability ratio of $^{90}$Zr$(p,p'n)$ decreases with increasing $L$ value.

### C. $J$ dependence around $S_n$

As predicted in [17], $P_i(E_x)$ for $^{90}$Zr is expected to show a significant $J$ dependence around $S_n$ due to the low level density in the neighboring nucleus, $^{89}$Zr. As shown in Fig. 3, the highest $J^\pi$ value in $^{89}$Zr is $9/2^+$ until the $J^\pi = 13/2^+$ state appears at $E_x = 1.943$ MeV. When a $J$ as high as 6–8 $\hbar$ was populated in $^{90}$Zr around $S_n$, neutron emission from those states are suppressed compared to neutron emission from $J$

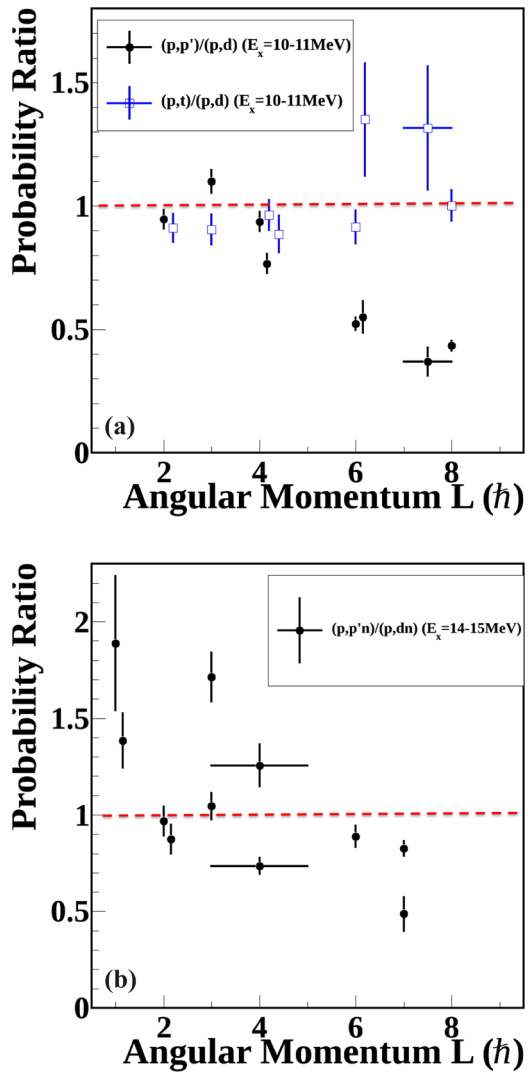


FIG. 6. (Color online) (a) $\gamma$ decay probability ratios of $^{90}$Zr$(p,p')$ and $^{92}$Zr$(p,t)$ to $^{91}$Zr$(p,d)$ at $E_x = 10.0$–$11.0$ MeV. (b) $\gamma$ decay probability ratios of $^{90}$Zr$(p,p'n)$ to $^{91}$Zr$(p,dn)$ at $E_x = 14.0$–$15.0$ MeV. Some other $\gamma$ transitions are displayed in addition to ones shown in Fig. 3: $E_\gamma = 2222$ keV $(6^+ \rightarrow 5^-)$ and 1051 keV $[(7,8) \rightarrow 8^+]$ from $^{90}$Zr for (a), and $E_\gamma = 356$ keV $(5/2^- \rightarrow 3/2^-)$, 1155 keV $(1/2^- \rightarrow 1/2^-)$, 1833 keV $(5/2^+ \rightarrow 9/2^+)$, 2121 keV $(13/2^- \rightarrow 9/2^+)$, and 2128 keV $[(7/2^+) \rightarrow 9/2^+]$ from $^{89}$Zr for (b) [27,31]. Error bars in the $x$ axis come from uncertainties in $J^\pi$ assignment. Uncertainties of $L$ in $E_\gamma = 1511$ and 2128 keV are assigned to $\pm 1\hbar$ for the present data analysis. Red dashed lines indicate unity.

states of 1–4 $\hbar$ because it requires high neutron energy to tunnel through the centrifugal barrier in $^{90}$Zr. The $P_i(E_x)$ for the high $J$ states are thus not expected to drop rapidly above $S_n$ until the excitation energy in $^{90}$Zr reaches $E_x = 13940$ keV corresponding to 1943 keV state in $^{89}$Zr.

Figure 7(a) and 7(b) show the $P_i(E_x)$ of $^{90}$Zr$(p,p')$ and $^{91}$Zr$(p,d)$ for the discrete $\gamma$ rays emitted from levels with $J = 2$, 4, 6, and 8 $\hbar$. Note that their $P_i(E_x)$ are normalized to unity below $S_n$ for convenience in comparison of the drop off above $S_n$ [the absolute values of $P_i(E_x)$ are already shown in Fig. 4]. These results show that $P_i(E_x)$ for the high $J$ states do not rapidly drop until the $13/2^+$ state at 1943 keV in $^{89}$Zr becomes energetically accessible. Thus $P_i(E_x)$ is very sensitive to $J$ and its dependence on $J$ around $S_n$ can be very useful for constraining the $J^\pi$ distribution of the compound nucleus as predicted by [17].

Garrett *et al.* [31] showed that for the $(n,n'\gamma)$ reaction, the population of high $J$ states increases with excitation energies while the population of low $J$ states decreases with $E_x$. An analogous trend is observed in $\gamma$-ray transitions from our $^{90}$Zr$(p,p'n)$ data. Figure 7(c) shows $P_i(E_x)$ from the levels with $L = 1$, 3, 6, and 7 $\hbar$ from $^{90}$Zr$(p,p'n)$ reactions. Note that the $P_i(E_x)$ are normalized to around 0.5 at $E_x = 15.0$ MeV for convenience in comparison. The energy dependence of the $P_i(E_x)$ are obviously dependent on $L$: the higher $J$ states are populated more at higher $E_x$ while the lower $J$ states decrease in population probability with increasing $E_x$. This supports the discussion given in [31].

### D. Angular dependence

The angular dependence of $P_i(E_x)$ can be useful in understanding the angular dependence of $J^\pi$ distributions which should be included in Eq. (1). Figure 8 shows the angular dependence of $P_i(E_x)$ from the $^{90}$Zr$(p,p')$, $^{91}$Zr$(p,d)$, and $^{92}$Zr$(p,t)$ reactions. These $P_i(E_x)$ were obtained from the $N_{\text{singles}}(E_x)$ and $N_{P\text{-}\gamma}(E_x,i)$ measured at three different particle scattering angular ranges of 25°–35°, 35°–50°, and 50°–60°, respectively, in the center-of-mass system ($\theta_{\text{c.m.}}$). The values plotted in Fig. 8 are average $P_i(E_x)$ values over $E_x = 10.0$–$11.0$ MeV.

Similar angular dependences are observed in the three different reactions. For example, the angular distributions for low $J$, i.e., $E_\gamma = 2186$ keV (from the level with $J = 2^+$) and $E_\gamma = 561$ keV (from $J = 3^-$), have a peak at 35°–50° except for the $E_\gamma = 561$ keV data from $^{92}$Zr$(p,t)$. And for $\gamma$ rays from the higher $J$ (4–8 $\hbar$), all the reactions have $P_i(E_x)$ which increases by factors of 2–3 with increasing angles.

Slight differences among $^{90}$Zr$(p,p')$, $^{91}$Zr$(p,d)$, and $^{92}$Zr$(p,t)$ reactions are still observable. The $(p,d)$ reaction seems to have the smallest angular dependence. To study the angular dependence in more detail, higher statistics are needed.

Figure 9 shows the angular dependence of the $\gamma$-ray transitions from the $^{90}$Zr$(p,p'n)$ reaction above the $S_n$. The $P_i(E_x)$ were obtained at $E_x = 14.0$–$15.0$ MeV. Just as in Fig. 8, the $P_i(E_x)$ for transitions from similar $J$ levels seem to have similar angular dependences, that is, the $P_i(E_x)$ from high $J$ levels such as 7$\hbar$ tend to continuously increase with increasing angle, and the $P_i(E_x)$ from low $J$ levels such as 1–4 $\hbar$ have a peak at 35°–50°.

## V. TOWARD THE APPLICATION TO THE SURROGATE REACTION APPROACH

Currently, theoretical efforts to obtain $(n,\gamma)$ cross sections from the surrogate reaction approach are under development [7]. These models require understanding the $J$ distribution populated in the compound nuclei. By comparing the measured absolute values of $P_i(E_x)$ with the calculated decay process, it is possible to deduce the $J^\pi$ distribution.

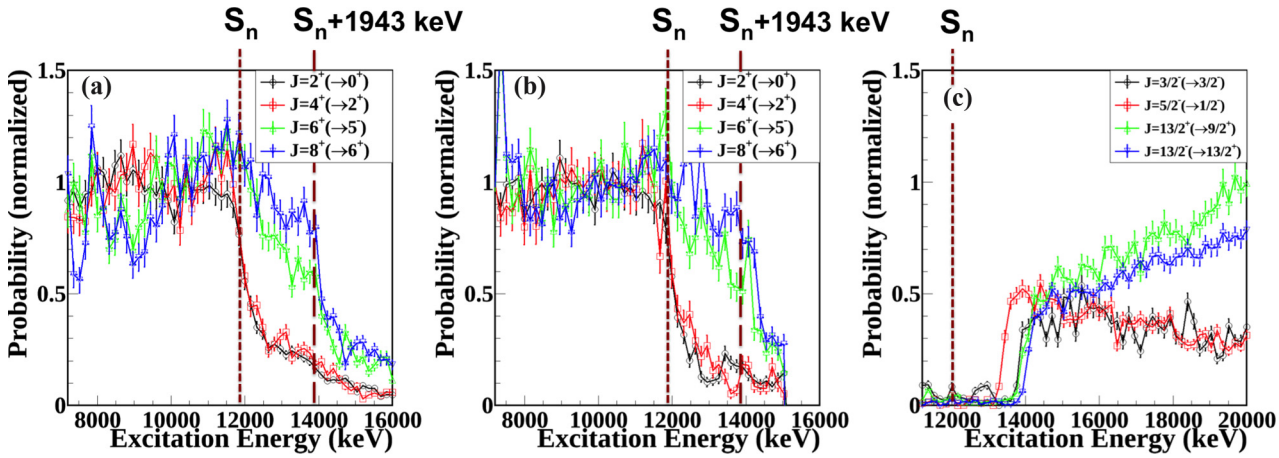


FIG. 7. (Color online) (a) $\gamma$ decay probabilities as a function of $^{90}$Zr excitation energy for $^{90}$Zr$(p,p')$, (b) $^{91}$Zr$(p,d)$, and (c) $^{90}$Zr$(p,p'n)$. Note these probabilities are normalized to 1, 1, and 0.5, respectively for convenience in comparison (see text for details). The $\gamma$-ray transitions shown are $E_\gamma = 2186$, 890, 1129, and 141 keV for (a) and (b), and $E_\gamma = 769$, 863, 1943, and 177 keV for (c).

Many experiments have shown a trend that the surrogate reactions tend to preferably populate higher $J$ than the direct measurements using neutron beams [15,20,23]. The present results indicate that $(p,p')$ populates much lower $J$ states than $(p,d)$ and $(p,t)$, therefore it is possible that $(p,p')$ provides a better surrogate for the direct measurements than $(p,d)$ and $(p,t)$ reactions. However, all these reactions show a strong angular dependence, so more sophisticated models are needed

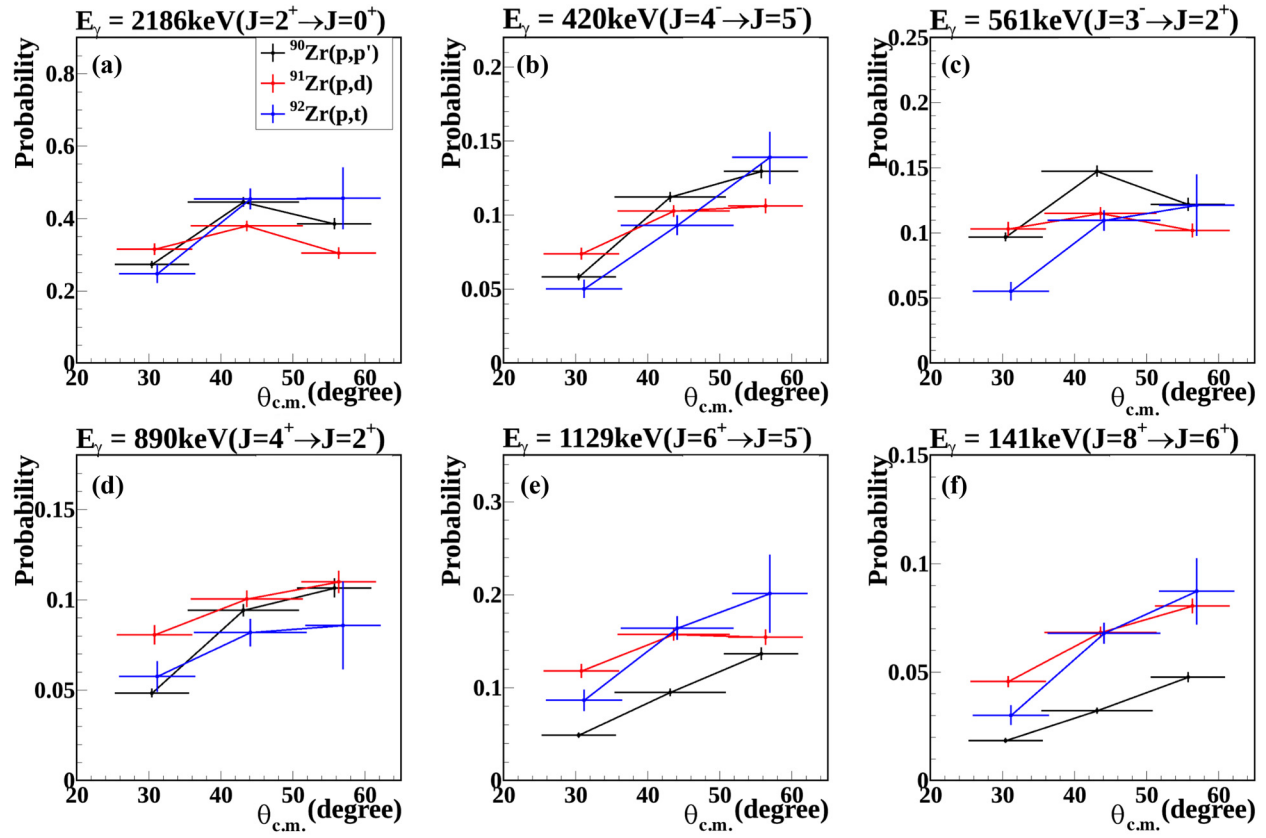


FIG. 8. (Color online) Angular dependence of $\gamma$ decay probabilities for the six intense $\gamma$-ray transitions from $^{90}$Zr$(p,p')$, $^{91}$Zr$(p,d)$, and $^{92}$Zr$(p,t)$ reactions. The probabilities are averaged at $E_x = 10.0$–$11.0$ MeV. (a) $E_\gamma = 2186$ keV, (b) 420 keV, (c) 561 keV, (d) 890 keV, (e) 1129 keV, and (f) 141 keV.

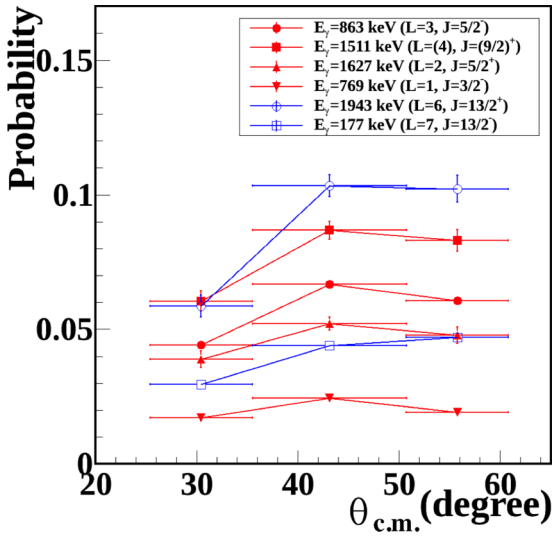


FIG. 9. (Color online) Angular dependence of $\gamma$ decay probabilities for six intense $\gamma$-ray transitions from $^{90}$Zr$(p,p'n)$ reactions. The probabilities are averaged at $E_x = 14.0$–$15.0$ MeV. $\gamma$-rays from levels with similar angular momentum are grouped in the same color (low $J$: red; high $J$: blue).

to account for the angular dependence and measurements with large particle angular acceptance are required. Furthermore, when a surrogate measurement via inelastic scattering is possible, a $(\gamma,\gamma')$ measurement might be possible. The latter has certain advantages, such as bringing in a well-defined angular momentum transfer and being able to provide information on the $\gamma$-ray strength function—an essential ingredients for $(n,\gamma)$ cross section calculations—with little need for modeling.

$(p,d)$, $(p,t)$, $(d,p)$, and $(d,t)$ reactions provide additional possibilities because they provide access to more neutron- or proton-rich compound nuclei just off of stability especially when used in inverse-kinematics experiments with radioactive beams. It is also interesting that the $(p,d)$ and $(p,t)$ reactions did not show notable differences in $P_i(E_x)$ for $J = 1$–$8\,\hbar$ states. This suggests that both reactions populate similar $J^\pi$ distributions. However, these two reactions are expected to have different reaction mechanisms because $(p,t)$, unlike $(p,d)$, is expected to be dominated by a two-step reaction. Therefore, more detailed investigation should be pursued. From the present data, the $(p,d)$ reaction shows a smaller angular dependence, making it a good approach when the experimental angular acceptance is limited.

Measurements that cover a large angular range for charged particles and $\gamma$ rays will be of significant help in collecting data needed to constrain theoretical models used to describe surrogate reactions. A silicon detector array with angular coverage of 10°–170°, called HYDRA, and a large Ge detector array for $\gamma$-ray measurements called HYPERION (utilizing the same Si telescope discussed in this work but coupled to up to 14 Compton suppressed HPGe clover detectors) [34], have been developed by the LLNL group. These arrays will be utilized in further investigation of the surrogate reaction approach.

## VI. CONCLUSION

The nucleus $^{90}$Zr was investigated with three different reactions: $(p,p')$, $(p,d)$, and $(p,t)$. The outgoing particles were detected in coincidence with $\gamma$ rays emitted by $^{89,90}$Zr. These surrogate reaction data can then be used to understand the decay of the compound nucleus formed in $^{89}$Zr$(n,\gamma)$. The $\gamma$ decay probabilities, $P_i(E_x)$, are key to develop theoretical models for determining radiative neutron capture cross sections using the surrogate reaction approach. We carried out measurements of $P_i(E_x)$ for $\gamma$ rays occurring in the decay of $^{90}$Zr nucleus produced near $S_n$ (11.97 MeV) via three different reactions. We observed that the $^{90}$Zr$(p,p')$ reaction produces notably fewer $\gamma$ rays from high $J$ states than the $^{91}$Zr$(p,d)$ and $^{92}$Zr$(p,t)$ reactions. This suggests the inelastic scattering preferably populates lower $J$ states in $^{90}$Zr than the transfer reactions. This reaction dependence holds over several MeV above $S_n$.

The same $J$ dependence of $P_i(E_x)$ around $S_n$ was confirmed in both $(p,p')$ and $(p,d)$ reactions. While the $P_i(E_x)$ from low $J$ levels drop rapidly to 0 just above the neutron separation energy, those from higher $J$ stay nearly constant and finally drop about 2 MeV above $S_n$. This is because neutron emission is inhibited due to the $J$ mismatch of the high $J$ states to low $J$ states in the daughter nucleus ($^{89}$Zr). This effect provides an additional constraint on the theoretical models to deduce the $J^\pi$ distribution.

The angular dependence of $P_i(E_x)$ for the $(p,p')$, $(p,d)$, and $(p,t)$ reactions were studied in the measured angular range of 25°–60°. For all these reactions, the $P_i(E_x)$ from high $J$ levels tend to increase with increasing angle, and the ones from low $J$ levels have peak intensities at 35°–50°. Variations of the $P_i(E_x)$ depending on angles cause a factor of two or three difference in the $P_i(E_x)$. The behavior of the $P_i(E_x)$ observed reflects the fact that the angular momentum transferred to the final nucleus in the surrogate reaction depends on the reaction mechanism as well as angle of the outgoing particle.

More quantitative discussions regarding the $J^\pi$ states of the $^{90}$Zr compound nucleus, combined with theoretical work, will be forthcoming.

## ACKNOWLEDGMENTS

We express our thanks to the cyclotron staff at Texas A&M University. This work was performed under the auspices of the U.S. Department of Energy by Lawrence Livermore National Laboratory under Contract No. DE-AC52-07NA27344. One of the authors, S.O. is supported by a JSPS Postdoctoral Fellowship for Research Abroad. Partial support through the U.S. Department of Energy's Topical Collaboration TORUS is acknowledged. We also thank Dr. T. Kawano (Los Alamos National Laboratory) for discussions regarding the interpretation of the particle spectrum.

[1] N. Colonna, Energy Env. Sci. **3**, 1910 (2010).
[2] T. Rauscher, P. Mohr, I. Dillmann, and R. Plag, Astrophys. J. **738**, 143 (2011).
[3] F. Käppeler, R. Gallino, S. Bisterzo, and A. Wako, Rev. Mod. Phys. **83**, 157 (2011).
[4] F. N. Mortensen, J. M. Scott, and S. A. Colgate, Los Alamos Sci. **28**, 38 (2003).
[5] M. Kreisler, in *Proceedings of Particle Accelerator Conference 2007* (IEEE, Piscataway, NJ, 2007), pp. 124–126, http://accelconf.web.cern.ch/AccelConf/p07/PAPERS/MOZBC01.PDF
[6] M. May *et al.*, Nuclear Forensics: Role, State of the Art, Program Needs, Technical Report, Nuclear Forensics Working Group of the American Physical Society's Panel on Public Affairs and the American Association for the Advancement of Science, 2008 (unpublished).
[7] J. E. Escher, J. T. Harke, F. S. Dietrich, N. D. Scielzo, I. J. Thompson, and W. Younes, Rev. Mod. Phys. **84**, 353 (2012).
[8] W. Younes and H. C. Britt, Phys. Rev. C **67**, 024610 (2003).
[9] J. E. Escher and F. S. Dietrich, Phys. Rev. C **74**, 054601 (2006).
[10] G. Kessedjian, B. Jurado, M. Aiche, G. Barreau, A. Bidaud, S. Czajkowski, D. Dassié, B. Haas, L. Mathieu, L. Audouin, N. Capellan, L. Tassan-Got, J. N. Wilson, E. Berthoumieux, F. Gunsing, Ch. Theisen, O. Serot, E. Bauge, I. Ahmad, J. P. Greene, and R. V. F. Janssens, Phys. Lett. B **692**, 297 (2010).
[11] J. J. Ressler, J. T. Harke, J. E. Escher, C. T. Angell, M. S. Basunia, C. W. Beausang, L. A. Bernstein, D. L. Bleuel, R. J. Casperson, B. L. Goldblum, J. Gostic, R. Hatarik, R. Henderson, R. O. Hughes, J. Munson, L. W. Phair, T. J. Ross, N. D. Scielzo, E. Swanberg, I. J. Thompson, and M. Wiedeking, Phys. Rev. C **83**, 054610 (2011).
[12] R. J. Casperson, J. T. Harke, N. D. Scielzo, J. E. Escher, E. McCleskey, M. McCleskey, A. Saastamoinen, A. Spiridon, A. Ratkiewicz, A. Blanc, M. Kurokawa, and R. G. Pizzone, Phys. Rev. C **90**, 034601 (2014).
[13] R. O. Hughes, C. W. Beausang, T. J. Ross, J. T. Harke, R. J. Casperson, N. Cooper, J. E. Escher, K. Gell, E. Good, P. Humby, M. McCleskey, A. Saastimoinen, T. D. Tarlow, and I. J. Thompson, Phys. Rev. C **90**, 014304 (2014).
[14] J. E. Escher and F. S. Dietrich, Phys. Rev. C **81**, 024612 (2010).
[15] N. D. Scielzo, J. E. Escher, J. M. Allmond, M. S. Basunia, C. W. Beausang, L. A. Bernstein, D. L. Bleuel, J. T. Harke, R. M. Clark, F. S. Dietrich, P. Fallon, J. Gibelin, B. L. Goldblum, S. R. Lesher, M. A. McMahan, E. B. Norman, L. Phair, E. Rodriquez-Vieitez, S. A. Sheets, I. J. Thompson, and M. Wiedeking, Phys. Rev. C **81**, 034608 (2010).
[16] N. D. Scielzo, J. E. Escher, J. M. Allmond, M. S. Basunia, C. W. Beausang, L. A. Bernstein, D. L. Bleuel, J. T. Harke, R. M. Clark, F. S. Dietrich, P. Fallon, J. Gibelin, B. L. Goldblum, S. R. Lesher, M. A. McMahan, E. B. Norman, L. Phair, E. Rodriguez-Vieitez, S. A. Sheets, I. J. Thompson, and M. Wiedeking, Phys. Rev. C **85**, 054619 (2012).
[17] C. Forssén, F. S. Dietrich, J. E. Escher, R. D. Hoffman, and K. Kelley, Phys. Rev. C **75**, 055807 (2007).
[18] R. Hatarik, L. A. Bernstein, J. A. Cizewski, D. L. Bleuel, J. T. Harke, J. E. Escher, J. Gibelin, B. L. Goldblum, A. M. Hatarik, S. R. Lesher, P. D. O'Malley, L. Phair, E. Rodriguez-Vieitez, T. Swan, and M. Wiedeking, Phys. Rev. C **81**, 011602(R) (2010).
[19] S. Chiba and O. Iwamoto, Phys. Rev. C **81**, 044604 (2010).
[20] G. Boutoux, B. Jurado, V. Meot, O. Roig, L. Mathieu, M. Aïche, G. Barreau, N. Capellan, I. Companis, S. Czajkowski, K.-H. Schmidt, J. T. Burke, A. Bail, J. M. Daugas, T. Faul, P. Morel, N. Pillet, C. Theroine, X. Derkx, O. Serot, I. Matea, and L. Tassan-Got, Phys. Let. B **712**, 319 (2012).
[21] J. E. Escher, presented at CNR*13, 4th International Workshop on Compound-Nuclear Reactions and Related Topics, Maresias, Brazil, 2013 (unpublished).
[22] J. M. Allmond, L. A. Bernstein, C. W. Beausang, L. Phair, D. L. Bleuel, J. T. Harke, J. E. Escher, K. E. Evans, B. L. Goldblum, R. Hatarik, H. B. Jeppesen, S. R. Lesher, M. A. McMahan, J. O. Rasmussen, N. D. Scielzo, and M. Wiedeking, Phys. Rev. C **79**, 054610 (2009).
[23] T. J. Ross, C. W. Beausang, R. O. Hughes, J. M. Allmond, C. T. Angell, M. S. Basunia, D. L. Bleuel, J. T. Harke, R. J. Casperson, J. E. Escher, P. Fallon, R. Hatarik, J. Munson, S. Paschalis, M. Petri, L. Phair, J. J. Ressler, N. D. Scielzo, and I. J. Thompson, Phys. Rev. C **85**, 051304(R) (2012).
[24] S. Ota, J. T. Burke, R. J. Casperson, J. E. Escher, R. O. Hughes, J. J. Ressler, N. D. Scielzo, I. J. Thompson, R. A. E. Austin, E. McCleskey, M. McCleskey, A. Saastamoinen, and T. Ross, EPJ Web Conf. **93**, 02001 (2015).
[25] S. R. Lesher, L. Phair, L. A. Bernstein, D. L. Bleuel, J. T. Burke, J. A. Church, P. Fallon, J. Gibelin, N. D. Scielzo, and M. Wiedeking, Nucl. Instrum. Methods Phys. Res., Sect. A **621**, 286 (2010).
[26] http://www.micronsemiconductor.co.uk
[27] National Nuclear Data Center website, http://www.nndc.bnl.gov
[28] J. T. Burke, J. E. Escher, R. J. Casperson, N. D. Scielzo, R. O. Hughes, J. J. Ressler, S. Fisher, R. A. E. Austin, S. Ota, M. McCleskey, A. Saastamoinen, E. Simmons, G. G. Rapisrada, H. I. Park, A. Starke, T. C. Salzillo, M. N. Maguire, R. I. Gonzales, N. J. Foley, B. L. Abromeit, W. F. McGrew, M. J. DeVanzo, and T. J. Ross, LLNL Internal Report 2015 (unpublished).
[29] J. B. Ball and C. B. Fulmer, Phys. Rev. **172**, 1199 (1968).
[30] J. B. Ball, R. L. Auble, and P. G. Roos, Phys. Rev. C **4**, 196 (1971).
[31] P. E. Garrett, W. Younes, J. A. Becker, L. A. Bernstein, E. M. Baum, D. P. DiPrete, R. A. Gatenby, E. L. Johnson, C. A. McGrath, S. W. Yates, M. Devlin, N. Fotiades, R. O. Nelson, and B. A. Brown, Phys. Rev. C **68**, 024312 (2003).
[32] S. Ota *et al.*, The 5th International Workshop on Compound-Nuclear Reactions and Related Topics [EPJ Web Conf. (to be published)].
[33] T. Kibedi, T. W. Burrows, M. B. Trzhaskovskaya, P. M. Davidson, and C. W. Nestor, Nucl. Instrum. Methods Phys. Res., Sect. A **589**, 202 (2008).
[34] R. O. Hughes *et al.* (unpublished).